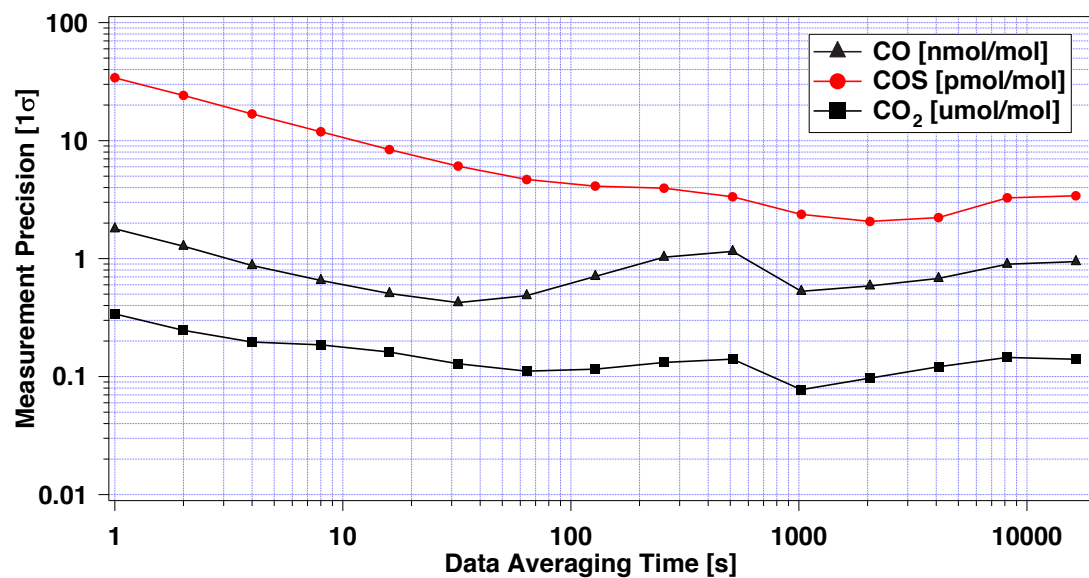


SUPP. FIGURES



SUPPLEMENTARY FIGURE 1. Allan Variance plot for the instrument running in a controlled laboratory environment with a reference tank as the gas source.

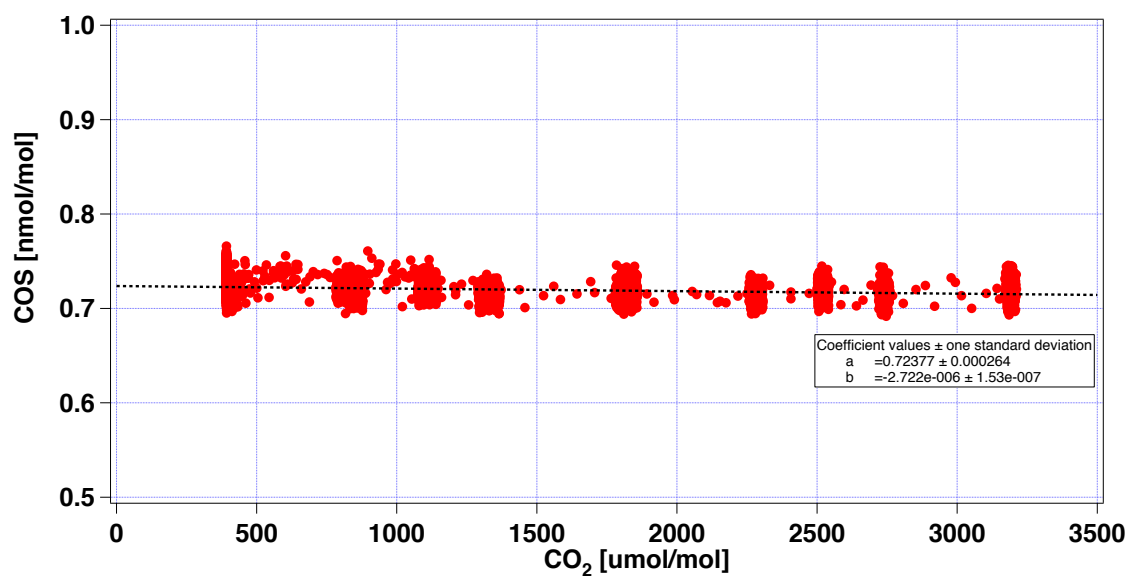


FIGURE 2. The response of the measured COS concentrations to increasing concentrations of CO₂ in the air. The slope of the fit is $-2.7e^{-3}$ pmol mol⁻¹ of COS for every $\mu\text{mol mol}^{-1}$ increase in CO₂, which is too small to detect given the range of the natural variations in ambient CO₂ concentrations observed.

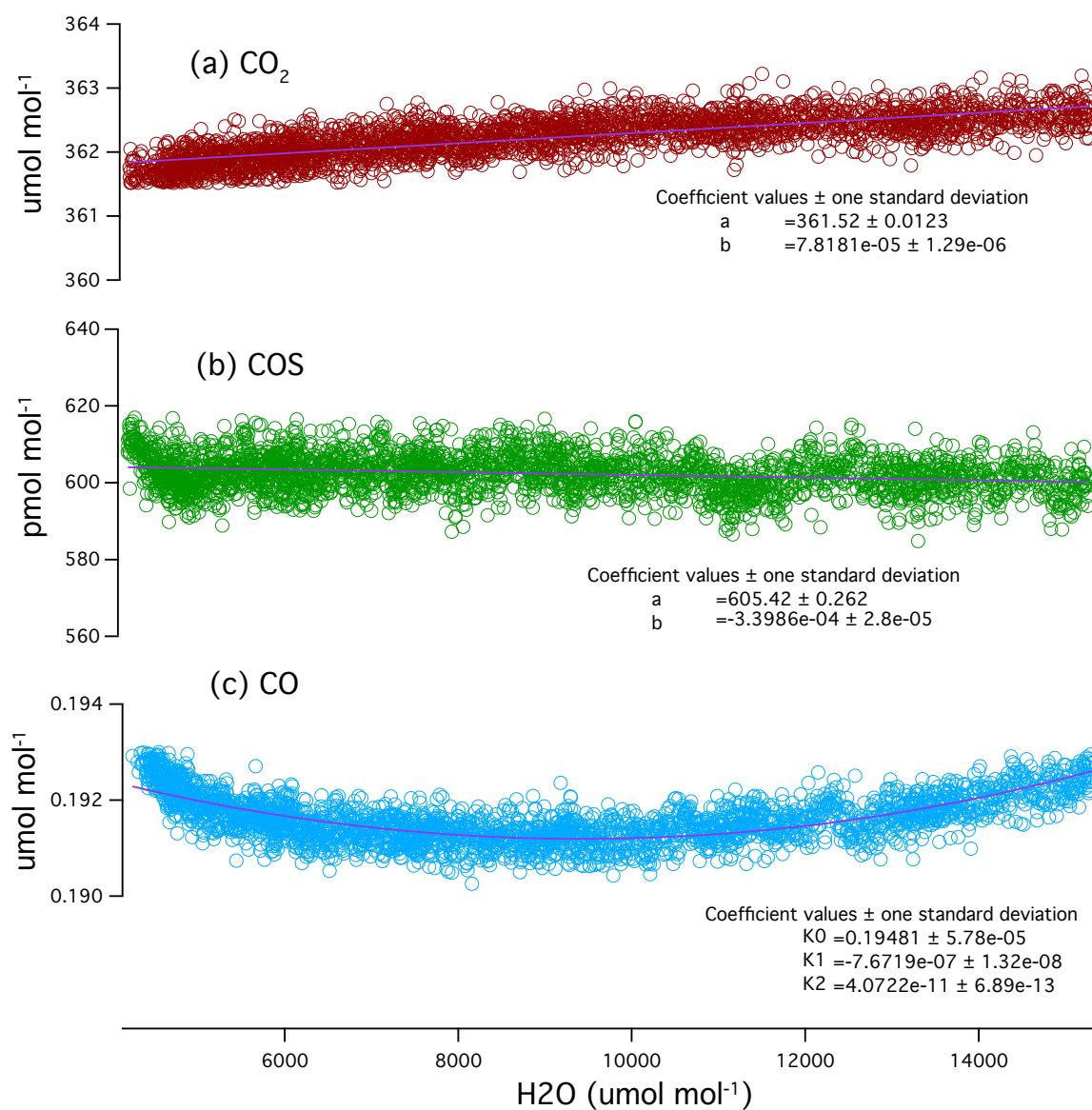


FIGURE 3. The response of COS, CO and CO_2 to increasing the water vapor concentration in the air sample. These data were generated in the lab through a dilution process. These data are shown after correction for water vapor is applied during the spectral analysis routine.

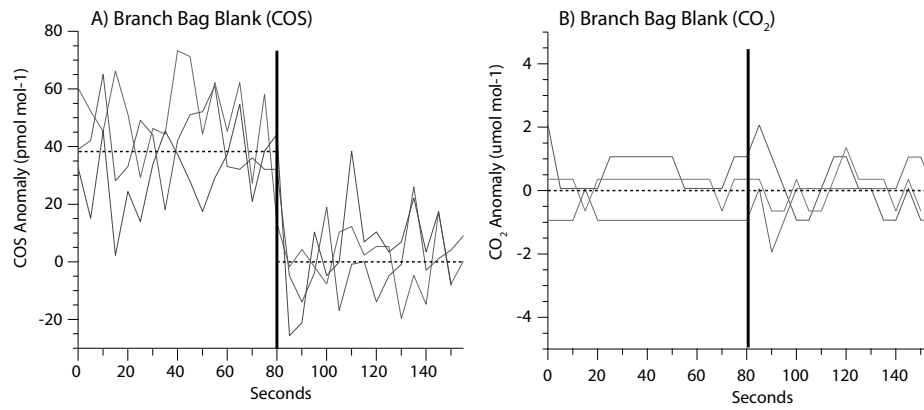


FIGURE 4. Blank analysis of the branch bag system. Three examples are shown for (a) COS and (b) CO₂ of switching between air passing through the branch bag and ambient air. No measurable change is found for CO₂ but an emission of $40 \text{ pmol mol}^{-1} \pm 8 \text{ pmol mol}^{-1}$ is found for COS, which is used to correct the flux values from the leaves.

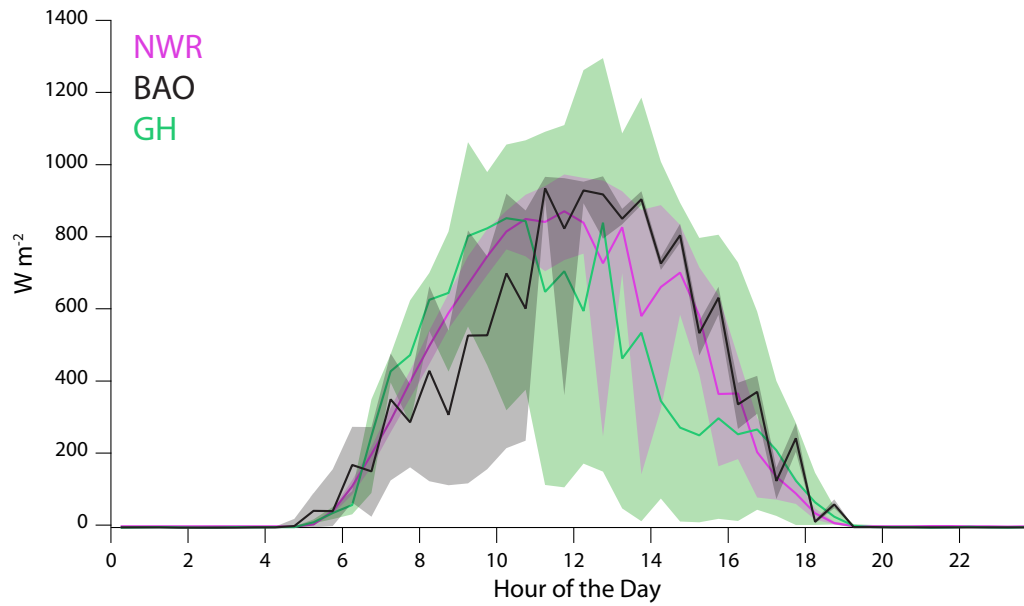


FIGURE 5. Downward shortwave radiation nearby the three sites from Kipp and Zonen radiometers at the BAO, University of Colorado Skywatch and Niwot Ridge LTER site. The shading encompasses the standard error based on the composite of all days at which measurements were made at the respective sites. The large variability is due to intermittent cloud cover.

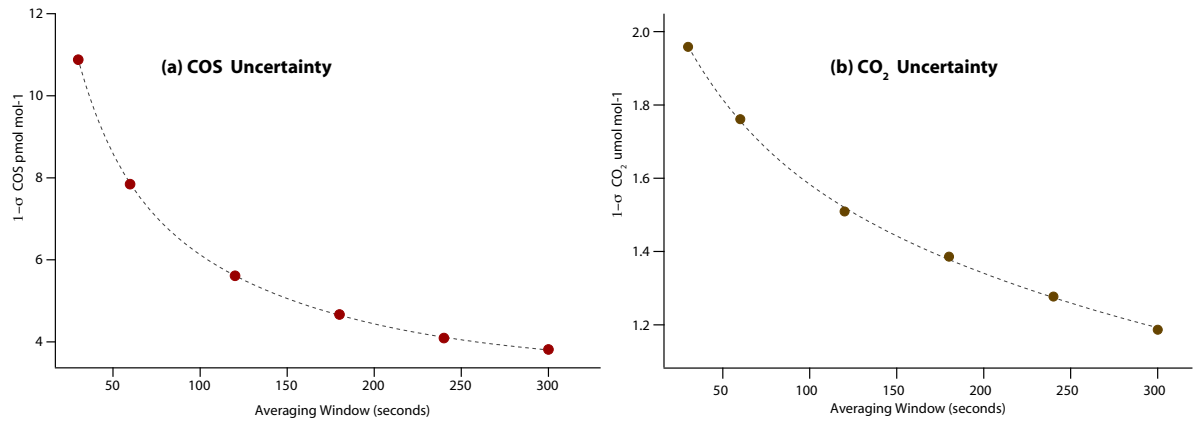


FIGURE 6. Standard deviation of (a) COS and (b) CO₂ as a function of increasing time window averaged. As opposed to Figure 1, this data was generated in the field using continuous injection of a reference gas over a multiple-hour period.

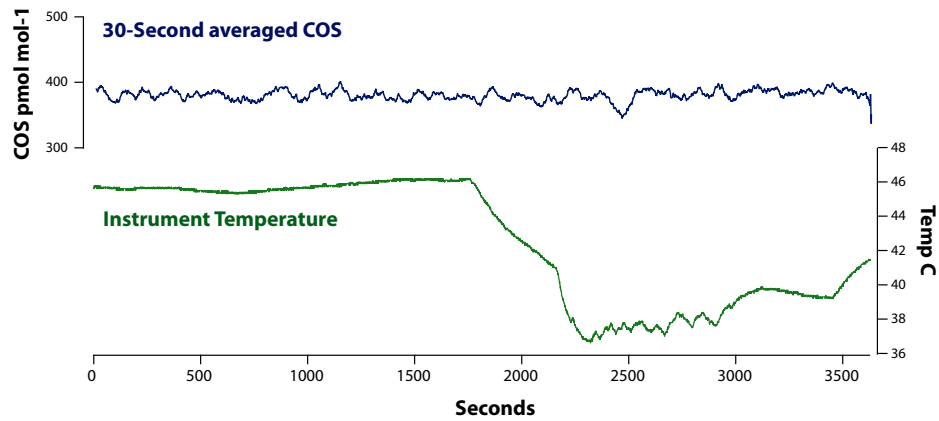


FIGURE 7. Measured COS concentrations and instrument temperature during a continued reference gas injection as ambient temperatures underwent a large change.

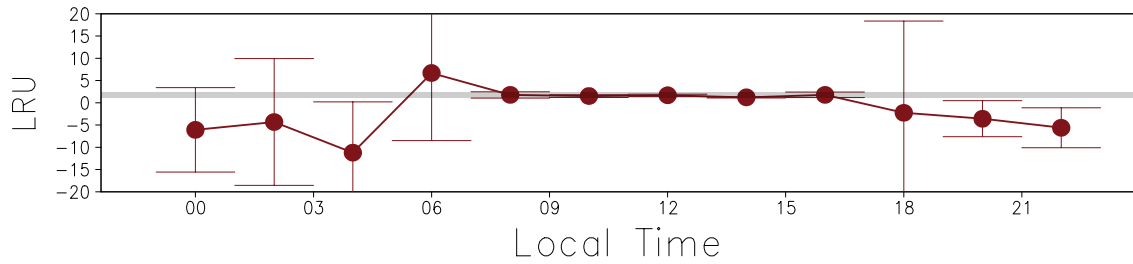


FIGURE 8. Leaf Relative Uptake (LRU) from the NWR site as a function of time of day. The gray bar indicates the average daytime LRU value at the site (1.7) and the error bars indicate the standard error based on repeat measurements. Measurements from both *populus tremuloides* and *pinus flexillis* were averaged together. The instability of LRU in the evenings arises because CO_2 (the denominator in Eqn. 2) approaches 0.

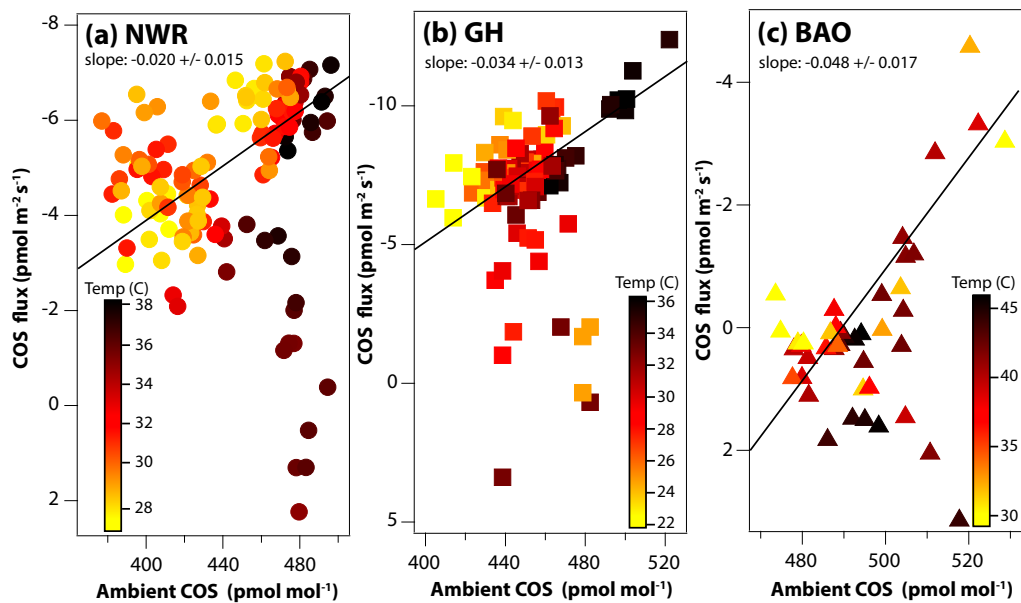


FIGURE 9. COS soil fluxes as a function of both chamber air temperature (colors) and ambient COS concentrations for (a) NWR, (b) GH and (c) BAO. Linear fits through the soil chambers measurements when uptake (as opposed to emission) occurred are shown as the black lines and the slopes are denoted at the top of each panel.

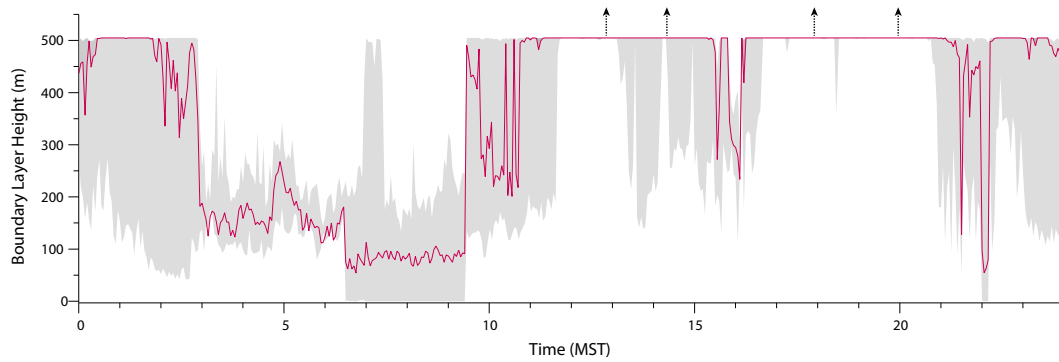


FIGURE 10. Approximate Boundary Layer Height derived from the SODAR at the BAO site (Coulter and Kallistratova, 2004). This is an example of a diel cycle for one day of the campaign where raw reflectivity was gridded on a 1 meter height resolution. The gray uncertainty envelope represents the maximum and minimum values at each time step by looking at all the days over a week long period and the arrows indicate periods when the boundary layer height was likely significantly higher but could not be resolved from the SODAR. Between 9 and 10 is when entrainment is the dominant influence on the COS and CO₂ concentrations and this corresponds to the rapid boundary layer growth seen here.

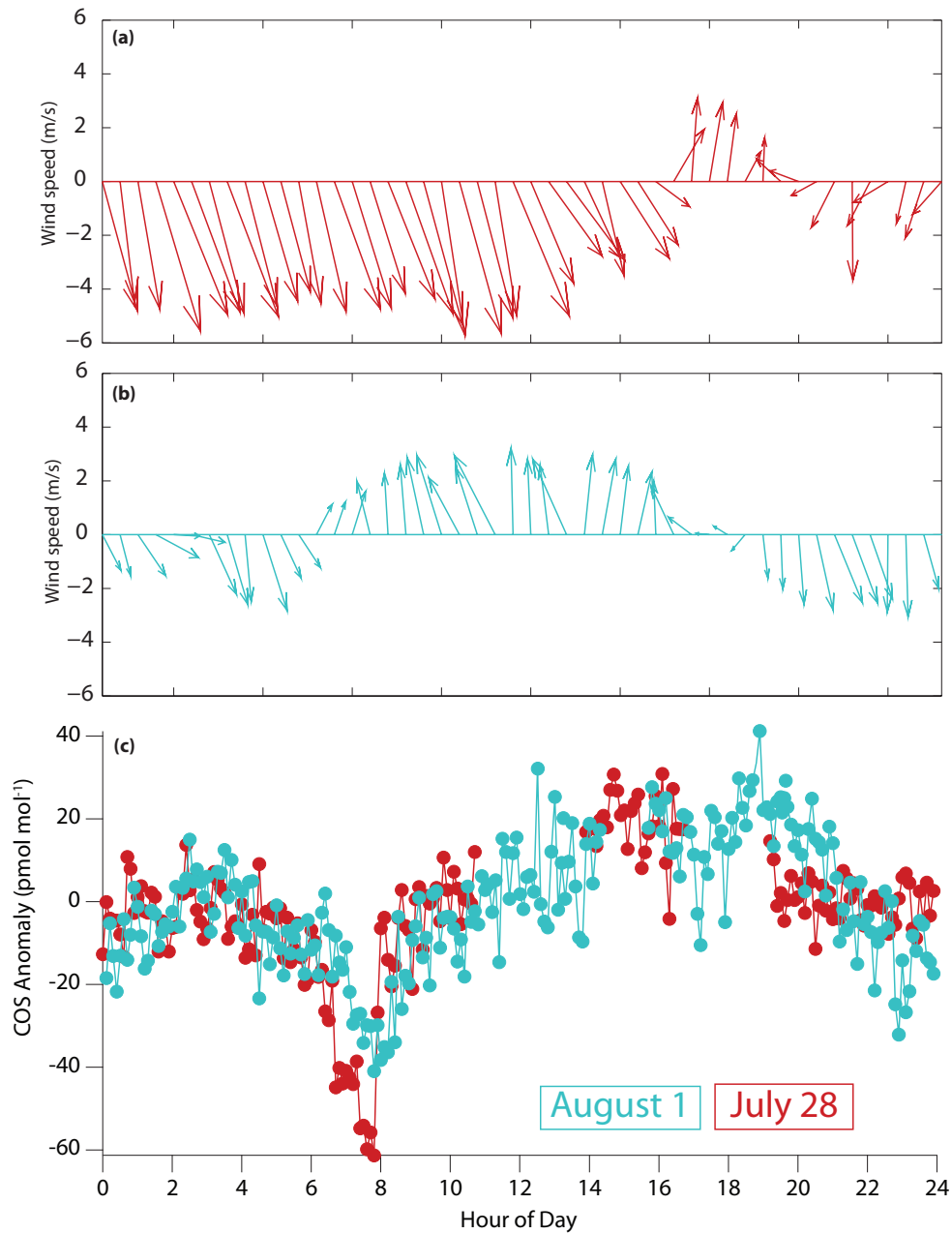


FIGURE 11. (a-b) Wind vectors for two days at the GH site. Panel A captures a day of principally upslope winds while Panel B captures a day with a strong transition between upslope and downslope winds. (c) Corresponding diel cycles in COS for the days shown in Panels A and B.